# Numerical Study of the Coupling Between Reaction and Mass Transfer for Liquid-Liquid Slug Flow in Square Microchannels

**Nathalie Di Miceli Raimondi and Laurent Prat**
Université de Toulouse; INPT, UPS; Laboratoire de Génie Chimique CNRS UMR 5503; 5 rue Paulin Talabot, BP1301, F- 31106 Toulouse cedex 01, France

*DOI 10.1002/aic.12411*
*Published online November 2, 2010 in Wiley Online Library (wileyonlinelibrary.com).*

*While the benefits of miniaturization on processes have been widely demonstrated, its impact on microfluidics and local mechanisms such as mass transfer is still little understood. The coupling between reaction and mass transfer in microchannels is simulated for liquid-liquid slug flow. First, the extrapolation to confined flow of the classical model used to calculate interfacial mass fluxes in reactive infinite media was studied. This model consists in estimating transferred fluxes between two phases as a function of the enhancement factor* E. *Its expression depends on the model used to represent interfacial mass transfer. In infinite media, Lewis and Whitman's stagnant film theory is generally preferred for its simplicity and its reliability. In the case of confined slug flow, the limitation of such a model to predict interfacial fluxes is highlighted. Second, the case of liquid-liquid competitive consecutive reactions in microchannels is considered. The unfavorable impact of the length between droplets on selectivity is emphasized. This is a direct consequence of mass-transport mechanisms in microchannels.* © 2010 American Institute of Chemical Engineers *AIChE J*, 57: 1719–1732, 2011
*Keywords: confined flow, liquid-liquid, mass transfer, reaction, simulations*

## Introduction

Process intensification by miniaturization opens up numerous perspectives in terms of chemical production. Indeed, decreasing device size allows a reduction of technology constraints to the benefit of chemistry.[1–3] On the one hand, microdevices are characterized by high-surface area to volume ratio, which provides them good thermal capacity.[4–6] On the other hand, it allows the enhancement of mass transfer notably in two-phase flow where high-interfacial area can be obtained.[7]

While the impact of miniaturization on such geometric parameter is well-known, its impact on microfluidics and local mechanisms such as mass transfer is still little understood. Consequently, to predict reaction results proceeded in a microchannel, many experiments are usually required. Hisamoto et al.[8] carried out a liquid-liquid diazocoupling reaction in a 20 mL stirred vessel (dispersed flow), and a microchannel (stratified flow).[8] For a conversion close to 100% in both devices, they observed the formation of precipitate side products at macroscale, while such precipitation did not appear at microscale. They mainly explained this unexpected phenomenon by mass-transfer enhancements due to short molecular diffusion distances that characterize microdevices. Wörz and et al.[1] used a micromixer coupled with a micro heat exchanger to carry out an exothermic liquid-liquid reaction.[1] They obtained higher conversion than in a feed-batch reactor, while diminishing by half the production of byproducts. These results are probably due to better mixing and thermal controls. These works confirm the potential of

Correspondence concerning this article should be addressed to N. D. M. Raimondi at nathalie.dimiceli@ensiacet.fr.

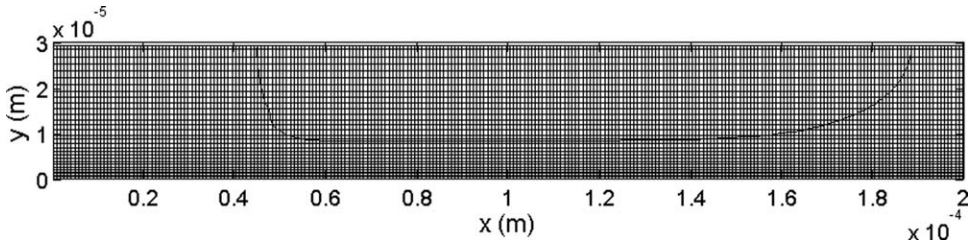


**Figure 1. Illustration of a 2-D computational mesh.**

The thick line represents the fictitious interface obtained with JADIM.

microtechnologies for chemical reaction, but highlight the complexity of fundamental mechanism coupling at microscale and the importance to acquire knowledge in this domain. Numerous research groups devoted their works on the coupling between hydrodynamics at microscale and mass transfer.[9–14] Fewer got interested in the comprehension of phenomenon coupling in two-phase reaction at such a scale.[15] This article focuses on the numerical study of the coupling between reaction and mass transfer in square microchannels considering liquid-liquid slug flow. This flow configuration is particularly interesting for mass transfer because of recirculation loops inside the droplets which intensify mixing in this phase,[16] and a film characterized by a high-velocity gradient which allows intense transfers with the droplets.[17] The study has been carried out as follows:

- First, the impact of reaction on liquid-liquid mass transfer is studied. Reaction can lead to an increase of interfacial mass-transfer fluxes.[18] This phenomenon is generally represented through the enhancement factor $E$, which is commonly used to estimate mass-transfer fluxes in infinite reactive media. The objective of this work is to study the extrapolation of this classical model to confined media.
- Second, this work deals with the impact of mass transfer on reaction. For that purpose, a competitive chemical scheme is considered to characterize the impact of mass transportation in liquid-liquid slug flow in microchannels on reaction selectivity.

### *Numerical method*

Two-dimensional (2-D) simulations are carried out to calculate the concentration field of a chemical component in a square microchannel. The computations are done in two steps: first, the hydrodynamic characteristics of the flow are determined using a research code developed at the Institute of Fluid Mechanics of Toulouse (IMFT-University of Toulouse, France): JADIM.[19] This code allows the resolution of continuity and Navier-Stokes equations in two-phase flows. The second step consists in the computation of the concentration field of the transferring component, based on the resolution of a mass balance for this component. This last code was developed under Matlab 7.4.

Tryggvason et al. pointed out the difficulty to compute the motion of multiphase flows.[20] The representation and simulation of deformable phase interfaces is still a major challenge. In their article, they reviewed the most popular numerical techniques used to compute Navier-Stokes equations in the case of multiphase flows. This work has led to a study on reactive mass transfer in bubbles.[21]

Volume-of-fluid method is used in this work. This numerical method is based on an interface-capturing technique without any interface reconstruction. The two-phase flow is described using the one-fluid approach. The phase tracking is insured by a continuous function $\phi$, the so called volume fraction, which equals zero in the continuous phase and one in the droplets: consequently, the interface is located in the area where $\phi$ strictly ranges from zero to one.[22] The equations and balances are discretized on space according to a finite-volume method.

This method assumes that (1) the fluids in both phases are Newtonian and incompressible, (2) the physical properties of both phases are constant and not influenced by mass transfer, (3) mass transfer has no impact on the flow (computation of the hydrodynamic parameters and the concentration field decoupled), and (4) the two-phase flow and the concentration are planar symmetric. Consequently, the computational domain is half a unit cell as shown in Figure 1. In the figure, the interface is fictitious (deduced from volume fraction as it is not calculated by JADIM code). The interface was arbitrary considered in the area where $\phi = 0.75$. This value was chosen since the concentration inside the droplets is important to identify mass-transfer coefficients in the droplet side from the concentration fields (this is described later). This choice has no impact on the computations.

JADIM code was previously validated to describe the hydrodynamics of liquid-liquid slug flow in square microchannels by means of particle image velocimetry (micro-PIV) experiments,[23] comparing computed and experimental 3-D velocity fields. Sarrazin et al.[23] also demonstrated that the hydrodymamic structure of slug flow in square microchannel could be well estimated using 2-D simulations.[23] Indeed, the velocity fields computed with JADIM performing 2- and 3-D simulations showed that the flow structures obtained with both kinds of simulation were similar. The purpose of this work is to identify a potential impact of channel size on the coupling between hydrodynamics, mass transfer and reaction. Since the hydrodynamics of liquid-liquid slug flow in microchannel is well represented by 2-D simulations, this work exclusively focuses on the calculation of hydrodynamic parameters and concentration fields over 2-D computational domains.

The whole numerical method was already used to study pure mass transfer in such two-phase systems.[13] The hydrodynamics and the concentration field computation algorithms are described in detail in this reference. This article will only present the mathematical formulation that allows the concentration field computation for chemical species that are

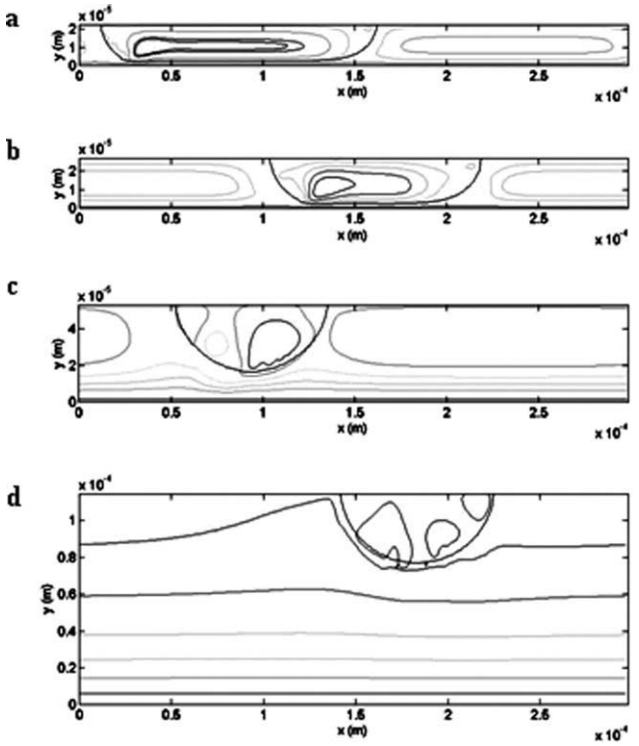


**Figure 2. Illustration of the streamlines in the flow configurations simulated to study the impact of reaction on mass transfer.**

(a) $L_d = 154.4$ $\mu$m, $w_C = 50$ $\mu$m, $U_d = 0.062$ m/s, $L_d/w_C = 3.1$, (b) $L_d = 121.6$ $\mu$m, $w_C = 60$ $\mu$m, $U_d = 0.039$ m/s, $L_d/w_C = 2.0$, (c) $L_d = 84.8$ $\mu$m, $w_C = 120$ $\mu$m, $U_d = 0.022$ m/s, $L_d/w_C = 0.71$, and (d) $L_d = 87$ $\mu$m, $w_C = 240$ $\mu$m, $U_d = 0.014$ m/s, $L_d/w_C = 0.36$.

affected by both mass transfer and reaction. This formulation depends on the reaction scheme and kinetic laws considered; therefore, it will be later described in each part dealing with a case study, that is, the study of the impact of reaction on mass transfer, and reciprocally.

### *Impact of reaction on mass transfer*

First, the impact of reaction on mass transfer is considered. The objective of this work is to study the extrapolation of the classical model used to estimate mass-transfer fluxes in reactive infinite media (i.e., based on the enhancement factor $E$ estimation) to confined media. The case of reactant A is considered, which transfers from the continuous phase to the dispersed phase and reacts to give product B

$$\mathrm{A} \rightarrow \mathrm{B} \qquad \text{in the dispersed phase} \tag{1}$$

This irreversible reaction is a first-order reaction whose kinetic rate $r_d$ is given by

$$r_d = KC_{d,A} \tag{2}$$

where $K$ is the kinetic rate constant of the reaction, and $C_{d,A}$ the concentration of A in the dispersed phase. The extrapolation of the classical model to confined media is studied comparing the mean concentration of reactant A in the droplets over time (1) obtained from concentration field computations (direct numerical simulations), and (2) estimated using the enhancement factor model. Four-flow configurations are considered, which present the same droplet volumes and the same unit cell lengths ($L_{UC} = 300$ $\mu$m), but different degrees of confinement as illustrated in Figure 2. This degree is represented by the ratio of the droplet length $L_d$, and the channel width $w_C$ ($L_d/w_C = 3.1$, 2.0, 0.71 and 0.36).

### *Concentration field computation*

The concentration field of component A over the computational domain is governed by the general convective diffusive equations in each phase, where the diffusive fluxes are expressed according to Fick's law

$$\frac{\partial C_{d,A}}{\partial t} + \mathbf{u}' \cdot \nabla C_{d,A} = D_{d,A}\nabla^2 C_{d,A} - KC_{d,A} \tag{3}$$

$$\frac{\partial C_{c,A}}{\partial t} + \mathbf{u}' \cdot \nabla C_{c,A} = D_{c,A}\nabla^2 C_{c,A} \tag{4}$$

where $t$ is the residence time. $\boldsymbol{u}'$ represents the velocity field in a frame of reference moving with the droplets. $D$ is the mass-diffusion coefficient of the transferring component. The subscripts $c$ and $d$, respectively, stand for the continuous and dispersed phases. It assumes the concentration at the interface obeys the thermodynamic equilibrium given by Eq. 5, $m$ being the distribution coefficient of component A between the two phases

$$C_{d,A} = mC_{c,A} \qquad \text{at the interface} \tag{5}$$

The resolution of Eqs. 3 and 4 according to the one-fluid approach requires the concentration to be continuous at the interface. For that purpose, some changes in the concentration formulation are suggested[24,25]

$$\hat{C}_{d,A} = C_{d,A}/\sqrt{m}, \hat{C}_{c,A} = C_{c,A}\sqrt{m} \tag{6}$$

Consequently, Eqs. 3, 4 and 5 can be rewritten as follows

$$\sqrt{m}\frac{\partial \hat{C}_{d,A}}{\partial t} + \sqrt{m}\mathbf{u}' \cdot \nabla \hat{C}_{d,A} = D_{d,A}\sqrt{m}\nabla^2 \hat{C}_{d,A} - K\sqrt{m}.\hat{C}_{d,A} \tag{7}$$

$$\frac{1}{\sqrt{m}}\frac{\partial \hat{C}_{c,A}}{\partial t} + \frac{1}{\sqrt{m}}\mathbf{u}' \cdot \nabla \hat{C}_{c,A} = \frac{D_c}{\sqrt{m}}\nabla^2 \hat{C}_{c,A} \tag{8}$$

$$\hat{C}_{d,A} = \hat{C}_{c,A} \qquad \text{at the interface} \tag{9}$$

Therefore, the mass balance in A over the whole computational domain can be represented by a single equation (Eq. 10), where $\hat{t}, \hat{\boldsymbol{u}}', \hat{D}$, and $\hat{K}$ are transformed parameters defined as a function of the volume fraction $\phi$ as shown by Eqs. 11–14. The concentration field is computed through the parameter $\hat{C}_A$

$$\frac{\partial \hat{C}_A}{\partial \hat{t}} + \hat{\boldsymbol{u}}' \cdot \nabla \hat{C}_A = \hat{D}\nabla^2 \hat{C}_A - \hat{K}\hat{C}_A \tag{10}$$

$$\hat{t} = \sqrt{m}t + \left(\frac{t}{\sqrt{m}} - \sqrt{m}t\right)\varphi \tag{11}$$

$$\hat{\boldsymbol{u}}' = \frac{\boldsymbol{u}'}{\sqrt{m}} + \left(\sqrt{m}\boldsymbol{u}' - \frac{\boldsymbol{u}'}{\sqrt{m}}\right)\varphi \tag{12}$$

$$\hat{D} = \frac{D_c D_d}{\varphi\left(D_c/\sqrt{m}\right) + (1-\varphi)D_d\sqrt{m}} \tag{13}$$

$$\hat{K} = \sqrt{m}K\varphi \tag{14}$$

### *Initial condition*

A is initially present in the continuous phase with a concentration $C_A^0$

$$\hat{C}_A = \sqrt{m}C_A^0(1-\varphi) \qquad \text{at } t = 0\,\text{s} \tag{15}$$

### *Boundary conditions*

At the wall and the symmetry plan, there is no mass flux over the direction normal to the flow

$$\frac{\partial \hat{C}_A}{\partial y} = 0 \quad \text{for} \quad y = 0 \quad \text{and} \quad y = w_C/2 \tag{16}$$

For the boundaries normal to the flow, two fictitious columns are introduced outside the domain to estimate the convective and diffusive terms. They are considered at the same concentration as the boundaries.

From the concentration field, the mean concentration profile of A in the droplets can be obtained using Eq. 17

$$\bar{C}_{d,A} = \frac{\iint \varphi C_d \cdot dxdy}{\iint \varphi \cdot dxdy} \tag{17}$$

### *Modeling of the mass-transfer enhancement phenomenon due to reaction*

The consumption of A during its transfer to the dispersed phase leads to a modification of the mass-transfer driving force, resulting in a mass-transfer enhancement phenomenon. This phenomenon is generally represented through the enhancement factor $E$.[26] The modeling of mass transfer with reaction is usually based on the Lewis and Whitman's stagnant film theory. This model is easy to apply and gives predictions in terms of transfer fluxes in reactive medium very close to those obtained using more sophisticated theories such as Higbie's penetration theory or Danckwerts' surface renewal model. Lewis and Whitman's stagnant film theory supposes that the interface is composed of two stagnant films which contain all the resistance to mass transfer. In this work, mass transfer is supposed to be at least limited by the resistance in the droplet side. Indeed, two distinct volumes contribute to mass transfer in the continuous phase: the film and the liquid slug between two droplets.[11] The importance of both contributions on interfacial mass-transfer kinetic is complex to determine. Previous works show that assuming mass transfer is partly limited by resistance in the droplet side allows good representation of mass fluxes at liquid-liquid interfaces in square microchannels of 50–960 $\mu$m depth.[13]

According to this model, the mass flux in reactive media transferring from the continuous phase to the droplets by interfacial area unit $(\Phi_m)_{c\to d}$ can be written in terms of Eq. 18. Its expression depends on the enhancement factor $E$

$$(\Phi_m)_{c\to d} = E \cdot k_d(C_d^i - C_d^b) \tag{18}$$

The superscripts $i$ and $b$, respectively, refers to the concentration at the interface and in the bulk phase. $k_d$ is the droplet mass-transfer coefficient. It is defined by Eq. 19, where $D_d$ is the mass-diffusion coefficient of the transferring component in the dispersed phase, and $\delta_d$ the stagnant film thickness

$$k_d = \frac{D_d}{\delta_d} \tag{19}$$

The mass balance at steady state for reactant A in the stagnant film (droplet side) can be written as follows

$$D_{d,A}\nabla^2 C_{d,A} + r_{d,A} = 0 \tag{20}$$

This equation relates the diffusive flux in the film, expressed in terms of Fick's law, and the flux consumed by reaction. There is no term relative to the convective flux because the film is supposed stagnant. Lewis and Whitman's theory considers that the mass-transfer flux between two phases is directed perpendicularly to the flow. Therefore, considering a 2-D representation of a square microchannel, Eq. 20 can be rewritten as follows

$$D_{d,A}\frac{d^2 C_{d,A}}{dy^2} = KC_{d,A} \tag{21}$$

In order to express Eq. 21 in a dimensionless form, changes of the variable on the concentration and the coordinate over the width are done (Eqs. 22 and 23). Thus, the mass balance in the stagnant film can be written in terms of Eq. 24

$$\chi_{d,A} = \frac{C_{d,A}}{C_{d,A}^i} \tag{22}$$

$$Y = \frac{y}{\delta_d} \tag{23}$$

$$\frac{d^2\chi_{d,A}}{dY^2} = \frac{K\delta_d^2}{D_{d,A}}\chi_{d,A} = \frac{KD_{d,A}}{k_{d,A}^2}\chi_{d,A} \tag{24}$$

In this equation appears the dimensionless Hatta number $Ha$, which represents the ratio of the maximal fluxes of reaction and of mass transfer

$$Ha^2 = \frac{KD_{d,A}}{k_d^2} \tag{25}$$

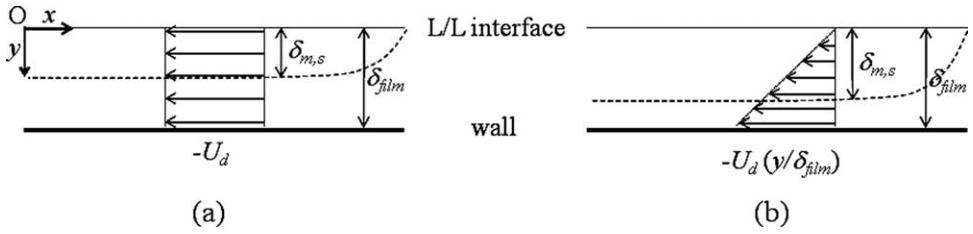


**Figure 3. Mean concentration profiles of *A* in the droplets, the continuous phase and at the interface, estimated from the simulations without reaction.**

(a) $L_d/w_C = 3.1$, (b) $L_d/w_C = 2.0$, (c) $L_d/w_C = 0.71$, and (d) $L_d/w_C = 0.36$.

### *Boundary conditions*

$$C_{d,A}(y=0) = C^i_{d,A} \Leftrightarrow \chi_{d,A}(Y=0) = 1 \quad \text{at the interface} \quad (26)$$

$$C_{d,A}(y=\delta_d) = C^b_{d,A} \Leftrightarrow \chi_{d,A}(Y=1) = \chi^b_{d,A} \quad \text{in the bulk} \quad (27)$$

The integration of Eq. 24 leads to an analytical solution. In accordance with the boundary conditions, this solution can be written as follows

$$\chi_{d,A} = \frac{1}{e^{Ha} - e^{-Ha}}\left[\chi^b_{d,A}\left(e^{Ha\cdot Y} - e^{-Ha\cdot Y}\right) + e^{Ha}\cdot e^{-Ha\cdot Y} - e^{-Ha}\cdot e^{Ha\cdot Y}\right] \quad (28)$$

Therefore, the mass-transfer flux at the interface can be expressed as a function of $Ha$

$$(\Phi_m)_{c\to d} = -D_{d,A}\left(\frac{dC_{d,A}}{dy}\right)_{y=0} = -k_d C^i_{d,A}\left(\frac{d\chi_{d,A}}{dY}\right)_{Y=0} = k_d\left(C^i_{d,A} - \frac{C^b_{d,A}}{\cosh(Ha)}\right)\frac{Ha}{\tanh(Ha)} \quad (29)$$

Finally, the enhancement factor $E$ is deduced from Eqs. 18 and 29

$$E = \frac{1}{\left(C^i_{d,A} - C^b_{d,A}\right)}\cdot\left(C^i_{d,A} - \frac{C^b_{d,A}}{\cosh(Ha)}\right)\frac{Ha}{\tanh(Ha)} \quad (30)$$

In this study, the mean concentration profiles of A in the droplets obtained from the concentration fields (Eq. 17) are compared to those calculated with mass balances on the droplets

$$V_d\frac{\partial \bar{C}_{d,A}}{\partial t} = (\Phi_{m,A})_{c\to d}a_d V_{UC} - K\bar{C}_{d,A}V_d \quad (31)$$

where $\overline{C}_{d,A}$ represents the mean concentration of A in the droplets. $V_d$ and $V_UC$, respectively, stand for the volumes of a droplet and a unit cell. $a_d$ is the specific interfacial area of the two-phase flow, estimated as a function of the capillary number.[13] The mass flux is calculated with Eqs. 18 and 30.

It assumes that the concentration of the bulk $C^b_{d,A}$ corresponded to the mean concentration in the droplet $\overline{C}_{d,A}$. This hypothesis has been chosen for this parameter is easier to experimentally capture than the concentration in the bulk. This assumption leads to an underestimation of the concentration gradient used to calculate interfacial mass flux. At macroscale, the impact of such an assumption is generally negligible as the stagnant film thickness is very small compared to the droplets diameter. At microscale, this assumption may strongly affect the mass-transferred flux estimation as it will be seen later.

The concentration at the interface $C^i_{d,A}$ was deduced from the concentration field computation. In the first unit cell, the concentration in both phases obeys the initial condition given by Eq. 15: the thermodynamic equilibrium at the interface is not imposed (Eq. 5). This leads to unrealistic value of the mean concentration of A at the interface on the first times of the operation. Consequently, the profiles obtained from computations and mass-balance calculations were compared from the second unit cell: time $t = 0$ on the graphs presented corresponding to a real residence time $t = T$, where $T$ is the flow period.

### *Results*

The extrapolation of the enhancement factor modeling to predict mass transfer in reactive media in microchannels is studied in two regimes defined by different Hatta number[27]

- $Ha = 0.1$: reaction is slow compared to mass transfer. Most of the reaction occurs in the bulk (within the droplets).
- $Ha = 1$: reaction- and mass-transfer rates are of the same order of magnitude. Part of the reaction occurs in the stagnant film.

When $Ha = 0.1$, the reaction is too slow to occur in the stagnant film and to induce a significant mass-transfer enhancement: $E$ is roughly equals to unity. Indeed, Danckwerts[28] presents values of enhancement factor as a function of Hatta number.[28] For a first-order reaction, $E$ is estimated at roughly 1.02 when $Ha = 0.1$, and 1.3 when $Ha = 1$. Consequently, the first part of the simulations does not lead to conclusions on the extrapolation of the enhancement factor modeling in microchannels. However, it will show whether the reaction flux in Eq. 31, calculated with an averaged concentration, reliably predicts the reactant consumption in the droplets.

Hatta number depends on the mass-transfer coefficient $k_d$ as shown in Eq. 25. For each flow configuration, this coefficient is first identified simulating pure mass-transfer operation, that is, without reaction. A prior study showed that the simulation results obtained with the numerical method used

**Table 1. Comparison Between the Estimated Thicknesses of the Concentration Boundary Layer and the Mesh Grid Sizes**

| | | | | |
|---|---|---|---|---|
| $L_d/w_C$ | 3.1 | 2.0 | 0.71 | 0.36 |
| $L_d$ ($\mu$m) | 154.4 | 121.6 | 84.8 | 87.0 |
| $\delta_{film}$ ($\mu$m) | 3.1 | 3.4 | 20.7 | 80.1 |
| $U_d$ (cm/s) | 6.16 | 3.68 | 2.21 | 1.44 |
| $\delta_{m,s}$ ($\mu$m) | 11.2 | 12.9 | 13.9 | 17.4 |
| $\Delta y$ ($\mu$m) | 0.3–1.33 | 0.3–1.65 | 0.3–3.47 | 1–2.97 |

in this work were affected by numerical diffusion.[13] This numerical diffusion corresponds to a truncation error of the convective term in the general mass-transport equation. This error is included in the apparent mass diffusion, leading to a global overestimation of the diffusive mass fluxes. In the simulated conditions, the numerical diffusion coefficient was estimated at about $4\times10^{-9}$ m$^2$/s, which is of the same order of magnitude as mass-diffusion coefficient in liquids (ca. $10^{-9}$ m$^2$/s). Hatta number is a function of the mass-diffusion coefficient. Therefore, this number numerically obtained from simulations will be underestimated by Eq. 25, which will affect the predictions of mass fluxes calculated using the enhancement factor $E$. In order to make the numerical diffusion impact negligible, a value of mass-diffusion coefficient was settled very high compared to the coefficient associated with numerical diffusion: $D = D_{d,A} = D_{c,A} = 5\times10^{-8}$ m$^2$/s.

In order to check the reliability of the computed concentration field near the interface, the thickness of concentration boundary layer $\delta_m$ is estimated and compared to the mesh grid size. Slip-boundary condition at the interface is assumed to minimize $\delta_m$. With such condition, velocity in the film is uniform, equal to $-U_d$ in the frame of reference moving with the droplets as illustrated in Figure 3 (the velocity profile in the film is linear when no-slip boundary condition is assumed).

The local equilibrium between mass diffusion and convection can be written as follows

$$u' \frac{\partial C}{\partial x} = -D \frac{\partial^2 C}{\partial y^2} \tag{32}$$

At the limit of the concentration boundary layer, both terms of Eq. 32 are approximated using characteristic parameters of the observed phenomenon

$$U_d \frac{\Delta C}{L_d} \approx D \frac{\Delta C}{\delta_{m,s}^2} \tag{33}$$

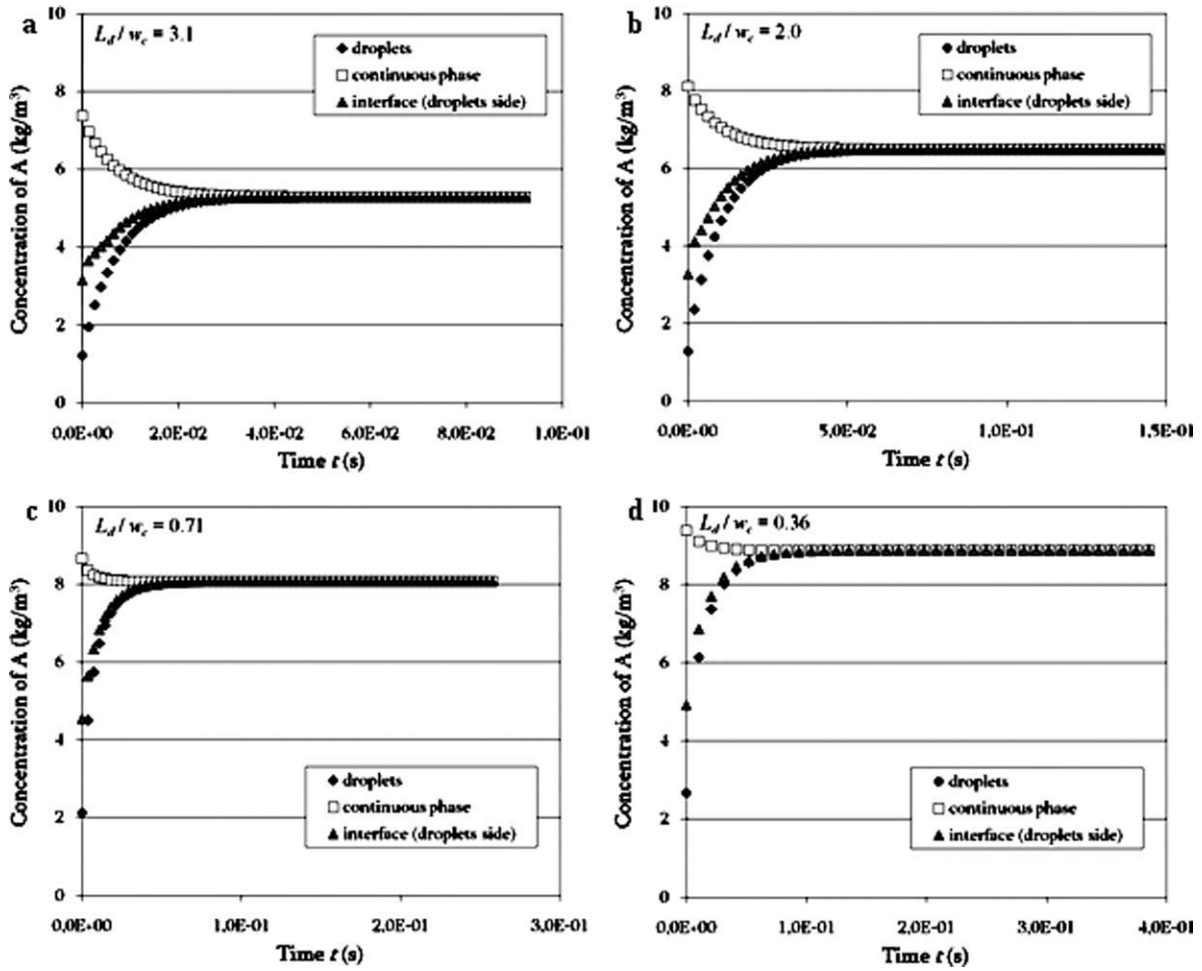


**Figure 4. Mean concentration profiles of *A* in the droplets simulated and calculated (without reaction).**

(a) $L_d/w_C = 3.1$, (b) $L_d/w_C = 2.0$, (c) $L_d/w_C = 0.71$, and (d) $L_d/w_C = 0.36$.

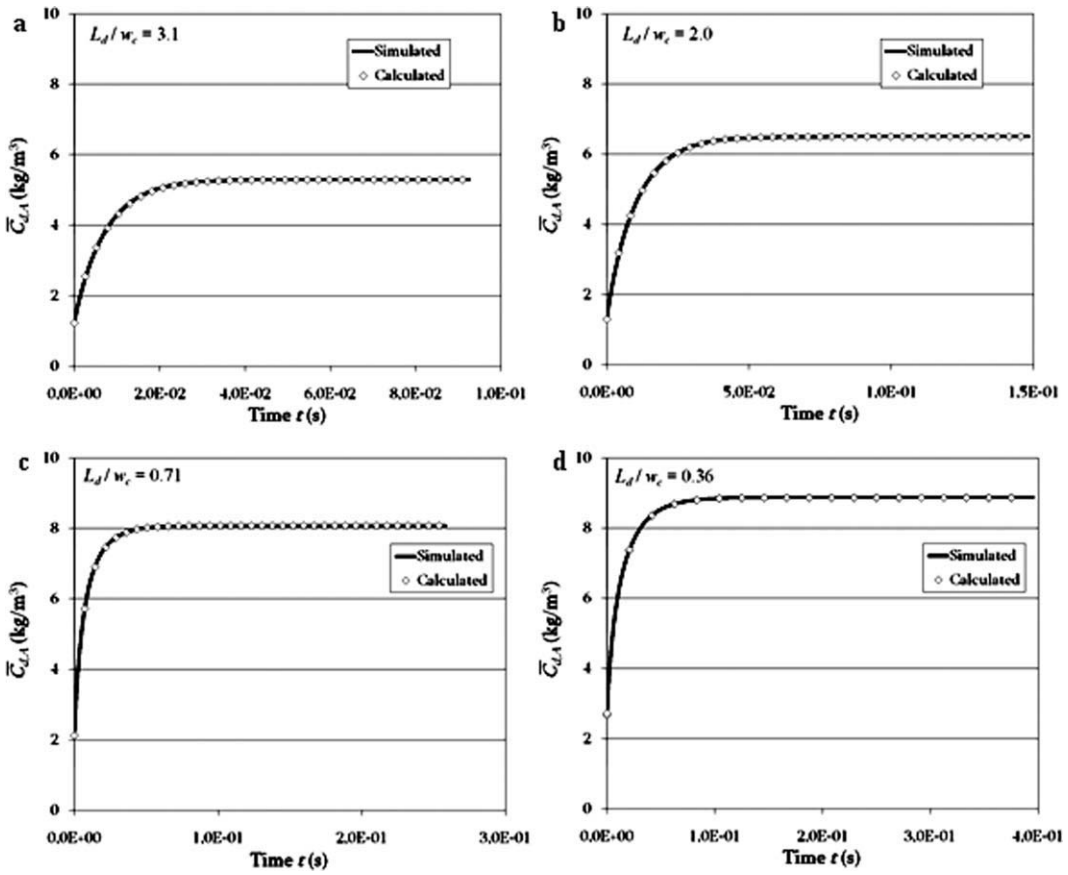


**Figure 5. Mean concentration profiles of *A* in the droplets simulated and calculated, *Ha* = 0.1.**

(a) $L_d/w_C = 3.1$, (b) $L_d/w_C = 2.0$, (c) $L_d/w_C = 0.71$, and (d) $L_d/w_C = 0.36$.

where $\delta_{m,s}$ is the thickness of concentration boundary layer assuming slip condition, and is estimated as a function of Peclet number $Pe$

$$\frac{\delta_{m,s}}{L_d} \approx \left(\frac{D}{U_d L_d}\right)^{1/2} = Pe^{-1/2}. \tag{34}$$

Table 1 shows the result of this layer estimation and the mesh grid size over the y-direction $\Delta y$ for the four-flow configuration used in this study. The mesh is refined near the wall: the smallest and highest mesh sizes are given. It is observed that the estimated thicknesses of the concentration boundary layer are higher than the mesh sizes. Therefore, grid refinement may be sufficient to predict mass transfer in this area.

Finally, the following parameters are used: $C_A^0 = 10$ kg.m$^{-3}$, and $m = 1$.

### *Identification of the mass-transfer coefficient without reaction*

The concentration field computation allows the calculation of the mean concentration profiles of A in the droplets, in the continuous phase and at the interface on the droplets side. Figure 4 shows these profiles for the four-flow configurations considered.

The concentration at an infinite time rises when the degree of confinement decreases, that is, when the channel diameter increases. This is logically due to the increase of the continuous phase volume, while the droplets volume and the initial concentration $C_A^0$ are the same in each flow configuration.

From the mean concentration in the droplets, the mass-transfer coefficient $k_d$ is identified so that the mass balance given by Eq. 35, and more precisely, the discretized form of Eq. 36, allows a good fitting of the mean concentration profile in the droplets obtained from the simulation

$$V_d \frac{\partial \bar{C}_{d,A}}{\partial t} = -k_d a_d V_{UC}\left(\bar{C}_{d,A} - \bar{C}^i_{d,A}\right) \tag{35}$$

$$\bar{C}_{d,A}(t+dt) = \bar{C}_{d,A}(t) - \frac{dt \cdot k_d a_d V_{UC}}{V_d}\left(\bar{C}_{d,A}(t) - \bar{C}^i_{d,A}(t)\right) \tag{36}$$

Figure 5 shows that the results of the identification are very satisfying. Indeed, the simulated profile and the one calculated from the mass balance present a good adequacy.

**Table 2. Mass-Transfer Coefficients Identified and Reaction Kinetic Constants Calculated to Study the Impact of Reaction on Transfer**

| $L_d/w_C$ | 3.1 | | 2.0 | | 0.71 | | 0.36 | |
|---|---|---|---|---|---|---|---|---|
| $k_d$ (m/s) | 3.06e-03 | | 3.03e-03 | | 5.29e-03 | | 3.35e-03 | |
| $Ha$ | 0.103 | 1.03 | 0.104 | 1.04 | 0.104 | 1.04 | 0.106 | 1.06 |
| $K$ (1/s) | 2 | 200 | 2 | 200 | 6 | 600 | 2.5 | 250 |

Table 2 presents the identified mass-transfer coefficient for each flow configurations studied. The values of the kinetic constant to set in the numerical code were determined in order to roughly obtain $Ha = 0.1$ and 1.

### *Impact of reaction on mass transfer, Ha = 0.1*

Figure 6 shows that the mean concentration profiles in the droplets obtained from the simulations are well predicted by Eq. 37, which is the discretized form of the mass balance given by Eq. 31. Indeed, the simulated and calculated profiles are very close whatever the degree of confinement of the droplets

$$\bar{C}_{d,A}(t+dt) = \bar{C}_{d,A}(t) - \frac{dt}{V_d} \cdot \left[ E \cdot k_d a_d \left( \bar{C}_{d,A}(t) - \bar{C}^i_{d,A}(t) \right) \times V_{UC} + K \bar{C}_{d,A}(t) \cdot V_d \right] \quad (37)$$

This result validates the reliability of the estimation of the reaction fluxes in Eq. 37 using a mean concentration over a droplet.

### *Impact of reaction on mass transfer, Ha = 1*

Finally, simulations are carried out with $Ha = 1$ in order to observe a significant impact of reaction on mass transfer. Figure 7 shows the comparison between the simulated and calculated concentration profiles in the droplets. This time, it is noticed an important difference between the two profiles.

This difference is more important in the confined flow configurations as illustrated in Figure 8, which represents the relative deviation between the two profiles as a function of the length in the microchannel. When droplets are confined ($L_d/w_C > 1$), the deviation is of about 35%, while it is

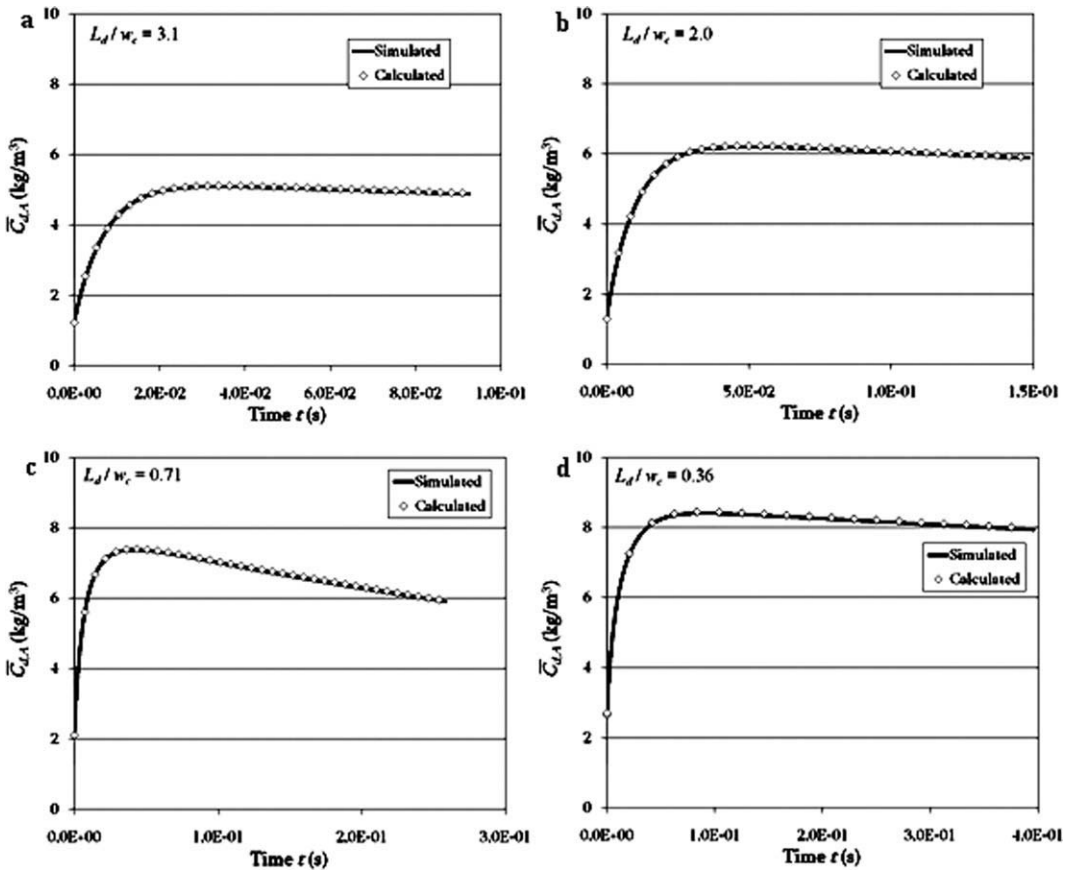


**Figure 6. Mean concentration profiles of *A* in the droplets simulated and calculated, *Ha* = 1.**

(a) $L_d/w_C = 3.1$, (b) $L_d/w_C = 2.0$, (c) $L_d/w_C = 0.71$, and (d) $L_d/w_C = 0.36$.

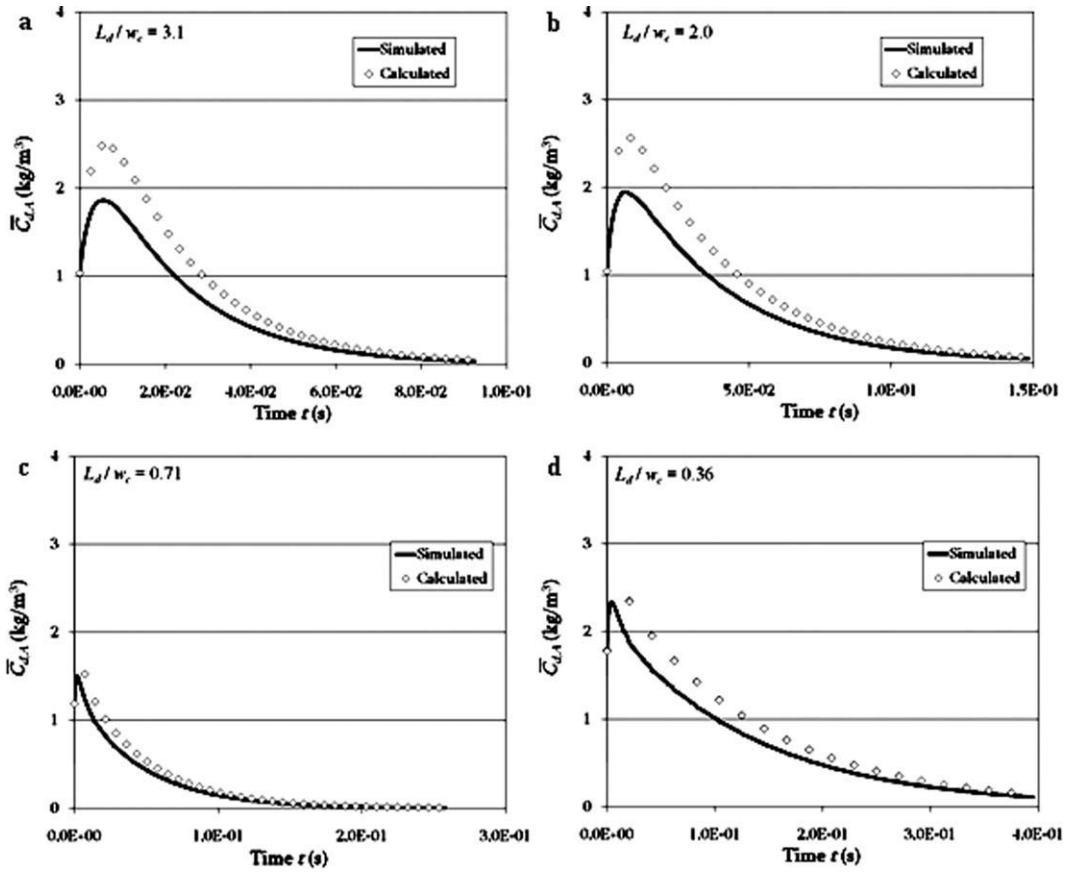


**Figure 7. Relative deviation between the simulated and calculated mean concentration profiles in the droplets as a function of the degree of confinement of the flow.**

roughly of 25% when $L_d/w_C < 1$. Moreover, it can be noticed that the calculated concentration profile overestimates the one obtained from the computations. This remark highlights that interfacial mass fluxes are overestimated by the model based on the enhancement factor calculation.

Indeed, concentration of the bulk in the droplet was approximated by the mean concentration in this volume. This implies an overestimation of the concentration gradient, and so an underestimation of the mass-transfer coefficient $k_d$ (see the section entitled Identification of the mass transfer coefficient without reaction) to compensate. This coefficient was used to calculate Hatta number as described by Eq. 25. Therefore, the classical model for the estimation of interfacial mass flux in reactive liquid-liquid media applied at microscale tends to an overestimation of Hatta number, and so of the enhancement factor which directly impacts on the prediction of mass fluxes.

### *Impact of mass transfer on reaction selectivity*

In the second part, the study focuses on the case of a complex chemical scheme to carry out in a microchannel. Consecutive competitive reactions given by the following scheme are considered

$$\text{R1}: \ \text{A} + \text{B} \rightarrow \text{C} \qquad \text{in the continuous phase} \qquad (38)$$

$$\text{R2}: \ \text{A} + \text{C} \rightarrow \text{D} \qquad \text{in the continuous phase} \qquad (39)$$

R1 and R2 are irreversible and second-order reactions whose respective kinetic rates $r_{c,1}$ and $r_{c,2}$ are given by

$$r_{c,1} = K_1 C_{c,A} C_{c,B} \qquad (40)$$

$$r_{c,2} = K_2 C_{c,A} C_{c,C} \qquad (41)$$

The reactants and products are soluble in both phases, but the reactions are supposed to occur only in the continuous phase. The desired product is $C$, and $D$ the byproduct. In homogeneous systems, the selectivity of the reaction would depend on the ratio of the kinetic rate constants $K_1/K_2$, and the conversion of $B$. In two-phase systems, mass transfer is a supplementary factor influencing the selectivity. The production of $D$ depends on:

- the residence time of component $C$ in the continuous phase after its formation. This time is linked to the transfer rate of $C$ from the continuous phase to the droplets,
- the kinetic of the second reaction.

The unit cell length is one of the factors influencing the mass-transfer kinetics in microchannels.[13] Indeed, its increase slows down the transfer between the two phases. In this work, the influence of the unit cell length on the selectivity of the competitive consecutive reaction scheme is studied by

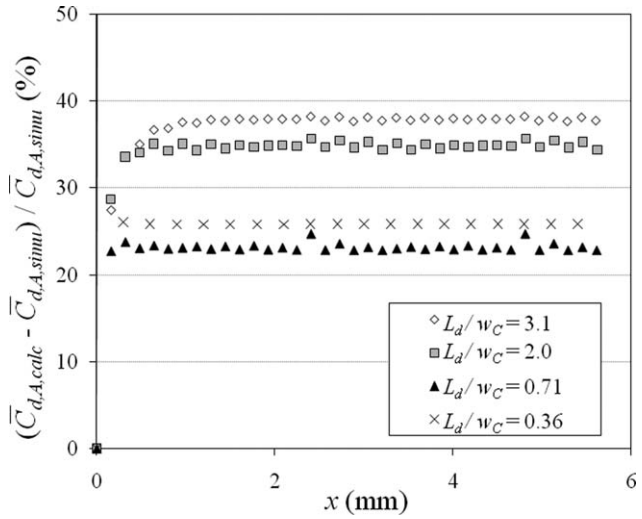


**Figure 8. Flow configurations simulated to study the impact of mass transfer on reaction selectivity.**

(a) $L_d = 100.8$ $\mu$m, $U_d = 0.15$ m/s, $w_C = 60$ mm, $L_{UC} = 300$ $\mu$m, and (b) $L_d = 100.8$ $\mu$m, $U_d = 0.15$ m/s, $w_C = 60$ mm, $L_{UC} = 600$ $\mu$m.

means of a numerical study based on the numerical tool described in the second part. The mathematical formulation of the mass balances has been modified to take into account the two reactions and to follow the concentrations of the four components. Two-flow configurations are considered, which present identical droplet length, velocity and hydrodynamic structures, but different unit cell length as it can be seen in Figure 9($L_{UC} = 300$ and 600 $\mu$m).

### *Mathematical formulation for the concentration field computation*

As previously mentioned, the reactions occur in the continuous phase. Consequently, the following mass balances and interfacial equilibrium for each component $j$ ($j$ corresponds to the species A, B, C or D), in both phases can be written as follows

$$\frac{\partial C_{d,j}}{\partial t} + \boldsymbol{u}' \cdot \nabla C_{d,j} = D_{d,j} \nabla^2 C_{d,j} \tag{42}$$

$$\frac{\partial C_{c,j}}{\partial t} + \boldsymbol{u}' \cdot \nabla C_{c,j} = D_{c,j} \nabla^2 C_{c,j} + \nu_{1,j} K_1 C_{c,A} C_{c,B} + \nu_{2,j} K_2 C_{c,A} C_{c,C} \tag{43}$$

$$C_{d,j} = m_j C_{c,j} \quad \text{at the interface} \tag{44}$$

where $\nu_{1,j}$ and $\nu_{2,j}$ stand for the stoichiometric coefficients of reactions R1 and R2. These equations were also formulated according to a one-fluid approach using the transformations described in the section entitled Concentration field computation. Simulations are done with $m_A = 1$, and $m_B = m_C = m_D = m$. The reactant A is initially present in the continuous phase (with a concentration $C_A^0 = 1$ kg/m$^3$), and B in the dispersed phase (with a concentration $C_B^0 = 10$ kg/m$^3$). Therefore, the reaction is initiated by the transfer of $B$ to the continuous phase.

### *Results*

The simulating conditions in terms of distribution coefficient $m$, and ratio of kinetic constants $K_1/K_2$ were varied. In order to highlight an impact of mass transport on reaction selectivity, kinetic constant values are set so that mass-transfer kinetics are not limiting compared to reaction kinetics. This avoids that the reactions strictly occur at the interface. For that purpose, the simulations were done at low Hatta number: $Ha < 0.5$.

*B, C and D Characterized by a High-Distribution Coefficient ($m = 500$), $K_1/K_2 = 10$* The distribution coefficient $m$ was set at 500, which means that B, C and D are preferentially present in the dispersed phase. This condition notably induces that the transfer of the reactant B is limited. The kinetic constant of the secondary reaction is 10 times lower than the one for the main reaction ($K_1 = 50$ m$^3$.mol$^{-1}$.s$^{-1}$; $K_2 = 5$ m$^3$.mol$^{-1}$.s$^{-1}$). Figure 10 illustrates the concentration fields obtained for each component at a residence time of 8 ms in the flow configuration characterized by the short unit cell length ($L_{UC} = 300$ $\mu$m). The color scale is not the same for each picture, but was adapted so that the concentrated areas for the different components clearly appear.

It is observed that:

- Concentration of $A$ tends to uniformity in both phase since this component is characterized by a distribution coefficient equal to unity.

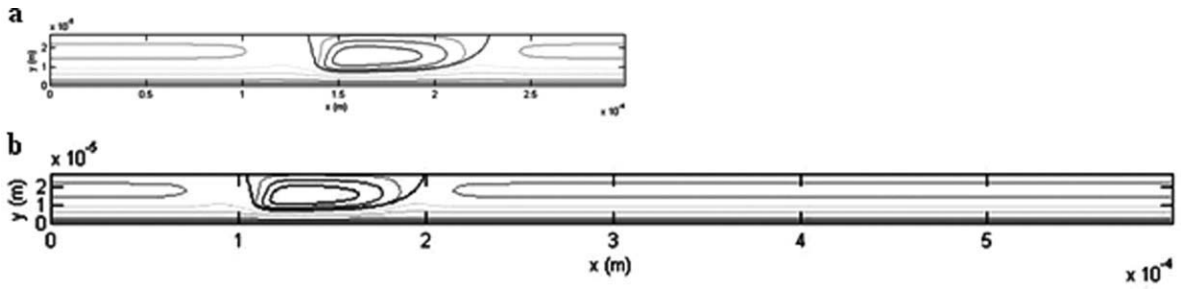


**Figure 9. Concentration fields of the reactants.**

(a) A and (b) B, and the products (c) C and (d) D at a residence time of 8 ms, $L_{UC} = 300$ $\mu$m, $m = 500$, $K_1 = 50$ m$^3$/(mol s), $K_2 = 5$ m$^3$/(mol s).

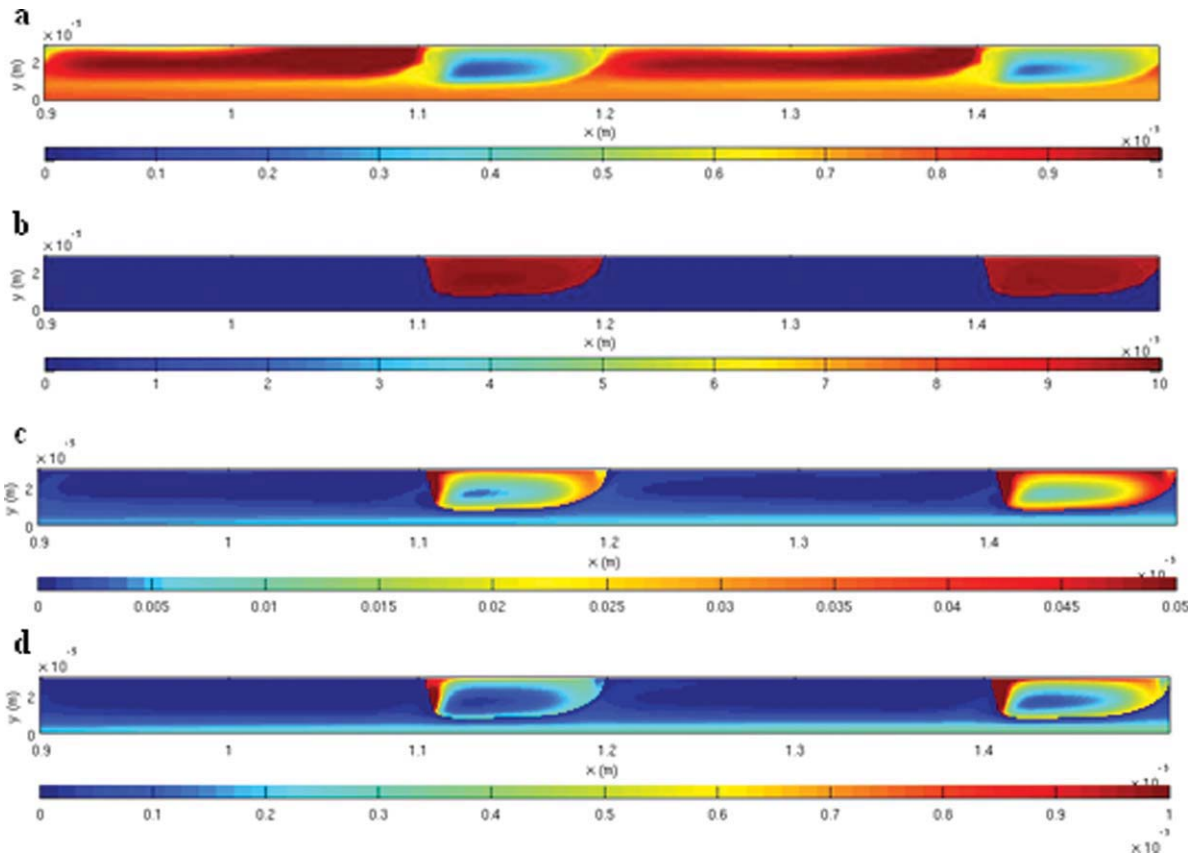


**Figure 10. Evolution of the selectivity for both flow configurations, $m = 500$, $K_1 = 50$ m$^3$/(mol s), $K_2 = 5$ m$^3$/(mol s).**

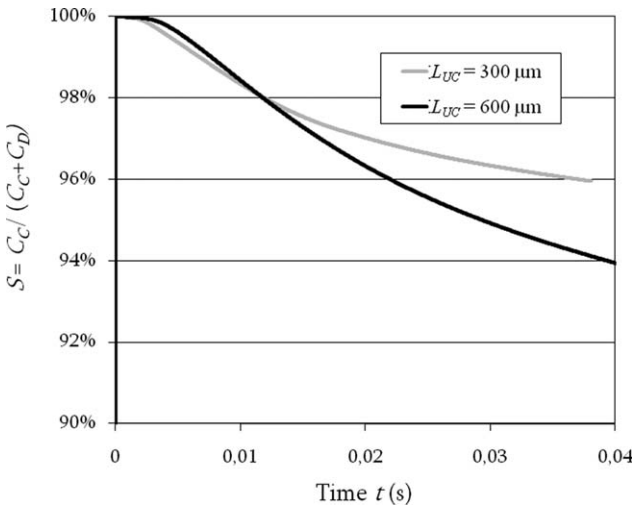


**Figure 11. Concentration field of byproduct *D* at a residence time of 8 ms, $L_{UC} = 300$ $\mu$m, $m = 500$, $K_1 = 50$ m$^3$/(mol s), $K_2 = 50$ m$^3$/(mol s).**

- Concentration of $B$ is much higher in the dispersed phase ($m = 500$): the mass-transferred fluxes of $B$ are low.
- Concentration of $C$ and $D$ are also higher in the dispersed phase ($m = 500$), while these components are produced in the continuous phase. It means that most of the reactions occur near the interface, which leads to a rapid transfer of these products to the dispersed phase after their generation.
- In the continuous phase, components $C$ and $D$ are in higher concentration in the film than in the interval, notably near the wall. This presumes that the reaction between $A$ and $B$ takes place dominantly in the film rather than in the interval. A small quantity of $C$ tends to accumulate in the film, which leads to a significant production of $D$ in this volume.

The same observations can be formulated on the concentration fields computed considering the flow configuration where $L_{UC} = 600$ $\mu$m.

From these concentration fields, selectivity of the reaction scheme $S$, defined in terms of Eq. 45, is calculated with the concentration of $C$ and $D$ averaged over a unit cell. Figure 11 illustrates $S$ for both flow configurations over time

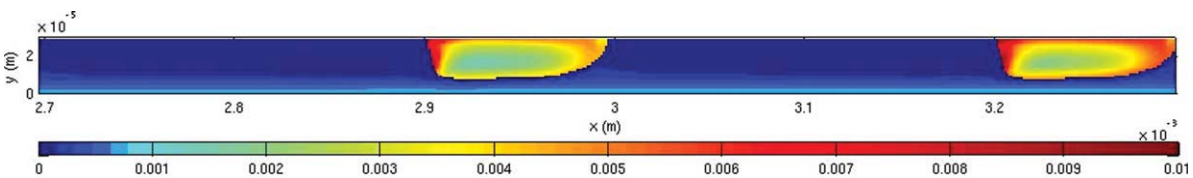


**Figure 12. Evolution of the selectivity for both flow configurations, $m = 500$, $K_1 = 50$ m$^3$/(mol.s), $K_2 = 50$ m$^3$/(mol.s).**

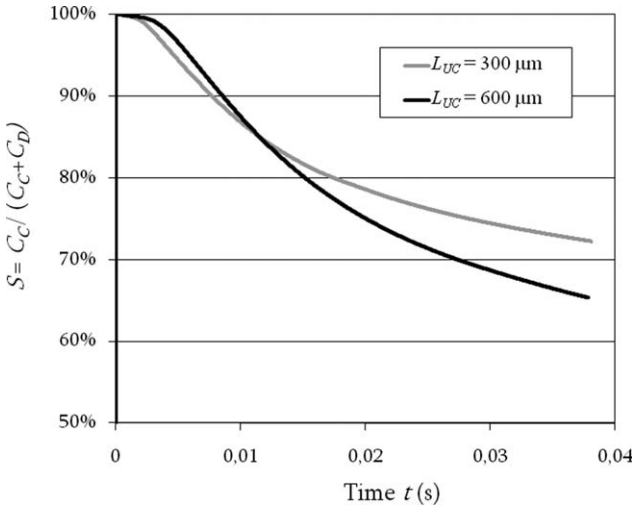


**Figure 13. Concentration fields of reactant (a) *A* and byproduct (b) *D* at a residence time of 8 ms, $L_{UC}$ = 300 $\mu$m, $m$ = 1, $K_1$ = 50 m$^3$/(mol s), $K_2$ = 5 m$^3$/(mol s).**

$$S = \frac{\bar{C}_C}{\bar{C}_C + \bar{C}_d} \tag{45}$$

During the first milliseconds, the selectivity's in both configurations are similar. However, then the selectivity in the case characterized by the shortest unit cell length becomes higher than in the other case. This is a direct consequence of the accumulation of $C$ in the film. Indeed, the longest the interval length, the highest the time available for $C$ to stray from the interface to the wall by diffusion through the film. This phenomenon disadvantages its transfer back to the dispersed phase in favor of its consumption by reaction 2.

Following this observation, the simulating conditions are modified with the idea to minimize the unfavorable impact of the unit cell length on the selectivity. For that purpose, two cases were investigated:

- First, the kinetic constant of the secondary reaction is increased ($K_2$ = 50 m$^3$.mol$^{-1}$.s$^{-1}$ $K_1/K_2$ = 1) in order to avoid the diffusion of product C toward the wall by enhancing its consumption by reaction 2.
- Second, the secondary reaction is limited in the film by impoverishing this volume in reactant A. For that purpose, the flux of $B$ was increased from the dispersed phase to the continuous phase by setting $m$ = 1. In order to assign the impoverishment of $A$ in the film to its consumption by reaction 1, it was set $K_1/K_2$ = 10. This is emphasized by the fact that $B$ is in large excess.

### *B, C and D characterized by a high-distribution coefficient ($m$ = 500), $K_1/K_2$ = 1*

The following parameters are set: $m$ = 500 and $K_1 = K_2$ = 50 m$^3$.mol$^{-1}$.s$^{-1}$. Figure 12 illustrates the concentration field of $D$ at a residence time of 8 ms in the flow configuration characterized by the short unit cell length ($L_{UC}$ = 300 $\mu$m).

This byproduct is again in high concentration near the wall: it is mainly formed in this area because of the diffusion of C through the film. In fact, despite the high value of $K_2$, the transfer of C to the wall is still significant since the low Hatta number was imposed. The results in terms of selectivity are similar to what was previously observed: the selectivity decreases when the interval length increases (Figure 13).

### *B, C and D characterized by a medium distribution coefficient ($m$ = 1), $K_1/K_2$ = 10*

Finally, the following parameters are set: $m$ = 1 and $K_1/K_2$ = 10 to observe an impoverishment of the reactant A in the film due to its consumption by reaction 1. This is illustrated on Figure 14a.

Indeed, this figure presents the concentration field of A at a residence time of 8 ms in the flow configuration characterized by the short unit cell length ($L_{UC}$ = 300 $\mu$m): it is observed a dark blue coloration of the film which is significant of poorly concentrated areas. However, byproduct D is still in high concentration near the wall (Figure 14b), which explains once again the negative impact of the unit cell length on the selectivity (Figure 15).

## Conclusion

In this work, the behavior of reacting liquid-liquid systems in microchannels was studied by means of numerical simulations. It aimed at underlining some issues relative to the proceeding of reaction in such systems, through two themes:

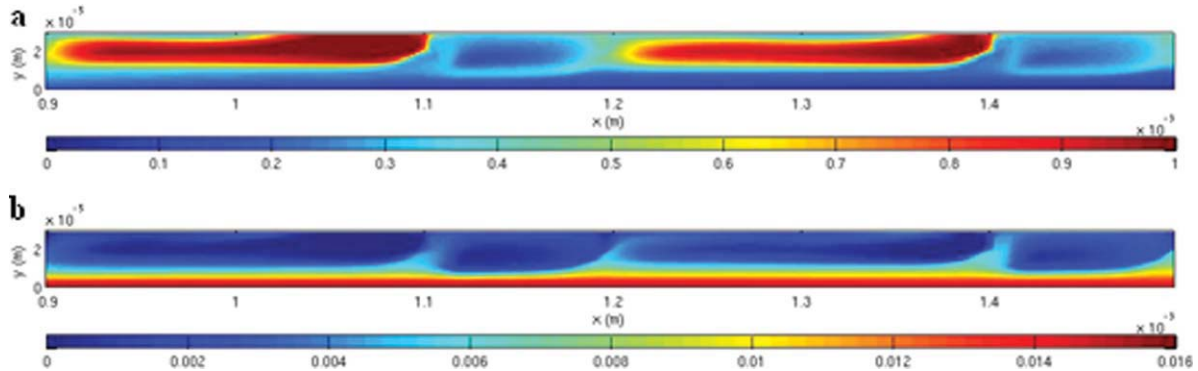


**Figure 14. Evolution of the selectivity for both flow configurations, $m$ = 1, $K_1$ = 50 m$^3$/(mol s), $K_2$ = 5 m$^3$/(mol s).**

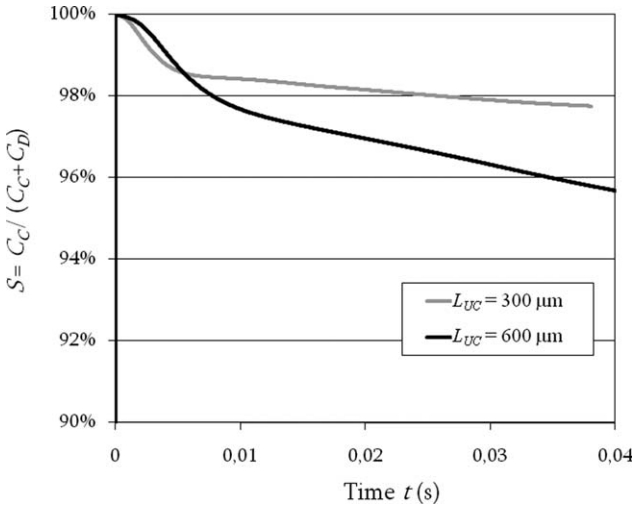


**Figure 15. Evolution of the selectivity for both flow configurations, $m = 1$, $K_1 = 50$ m$^3$/(mol s), $K_2 = 5$ m$^3$/(mol s).**

• First, the study focused on the modeling of mass transfer in reactive medium. Transfer fluxes between two phases are generally estimated as a function of the enhancement factor $E$. Its expression depends on the model used to represent interfacial mass transfer. In usual device, we generally refer to Lewis and Whitman's stagnant film theory for its simplicity and its reliability. In microchannels, it appeared that the enhancement factor was not well estimated considering such a model. Other theories such as Higbie's penetration theory could be more appropriated to represent interfacial transfer. In other words, this work shows that the way of apprehending mass transfer must take into account the degree of confinement of slug flows.

• Second, competitive consecutive reactions were considered in order to analyze the impact of the interval length between the droplets on the scheme selectivity. In the operating conditions simulated (low Hatta number), the selectivity tended to increase with a decrease of the unit cell length for a constant droplets length. This is due to the accumulation of the intermediate product $C$ near the wall by diffusion of this product from the interface through the film. This observation should be validated by an experimental study.

This last part also suggests that concentrations in reactants and intermediates products are not uniform in the microchannel, which raises the problem of hot spots formation when working with exothermic reactions. However, in our case (reactions occur in the continuous phase), the concentrated areas appear near the wall which is generally the region where the temperature control is optimal by heat exchange.

## Acknowledgments

This work has been supported by 6th Framework EU under Grant IMPULSE No: NMP2-CT-2005-011816 and the Institut National Polytechnique of Toulouse (see http://www.inp-toulouse.fr). Experiments presented in this article were carried out using the Grid'5000 experimental testbed, an initiative from the French Ministry of Research through the ACI GRID incentive action, INRIA, CNRS and RENATER and other contributing partners (see https://www.grid5000.fr).

## Notation

$a_d$ = specific interfacial area, m$^2$.m$^{-3}$
$C$ = concentration, kg.m$^{-3}$
$\overline{C}$ = mean concentration, kg.m$^{-3}$
$dt$ = time step, s
$D$ = mass-diffusion coefficient, m$^2$.s$^{-1}$
$E$ = enhancement factor
$k$ = mass-transfer coefficient, m.s$^{-1}$
$K$ = kinetic rate constant, s$^{-1}$, or m$^3$.mol$^{-1}$.s$^{-1}$
$L$ = length, m
$m$ = distribution coefficient
$r$ = reaction rate, kg.m$^{-3}$.s$^{-1}$
$S$ = selectivity
$t$ = time, s
$T$ = flow period, s
$\boldsymbol{u}$ = velocity vector, m.s$^{-1}$
$U$ = velocity, m.s$^{-1}$
$V$ = volume, m$^3$
$W$ = width, m
$x$ = coordinate over the length, m
$y$ = coordinate over the width, m
$Y$ = dimensionless coordinate over the width

### *Greek letters*

$\delta$ = stagnant film thickness, m
$\nu$ = stoichiometric coefficient
$\phi$ = volume fraction
$\Phi_m$ = mass-transfer flux by interfacial area unit, kg.m$^{-2}$.s$^{-1}$
$\chi$ = dimensionless concentration

### *Subscripts*

1 = reaction R1
2 = reaction R2
$A$ = component A
$B$ = component B
calc = calculated data
$C$ = component C
$d$ = dispersed phase or droplets
$D$ = component D
$j$ = chemical species, A, B, C or D
simu = data obtained from simulations
$UC$ = unit cell

### *Superscripts*

$0$ = at initial time
$b$ = bulk
$i$ = interface
$'$ = the frame of reference moving with the droplets
$\wedge$ = transformed parameter

## Literature Cited

1. Wörz O, Jäckel KP, Richter T, Wolf A. Microreactors, a new efficient tool for optimum reactor design. *Chem Eng Sci*. 2001; 56:1029–1033.
2. de Mello A, Wooton R. But what is it good for? Applications of microreactor technology for the fine chemical industry. *Lab Chip*. 2002;2:7N–13N.
3. Ahmed B, Barrow D, Wirth T. Enhancement of reaction rates by segmented fluid flow in capillary scale reactors. *Adv Synth Catal*. 2006;348:1043–1048.
4. Schubert K, Brandner J, Fichtner M, Linder G, Schygulla U, Wenka A. Microstructure devices for applications in thermal and chemical process engineering. *Microscale Thermophys Eng*. 2001;5(1):17–39.
5. Commenge JM, Falk L, Corriou JP, Matlosz M. Intensification des procédés par microstructuration. *C R Physique*. 2004;5:597–608.
6. Jähnish K, Hessel V, Löwe H, Baerns M. Chemistry in microstructured reactors. *Angew Chem Int*. 2004;43:406–446.
7. Yue J, Chen G, Yuan Q, Luo L, Gonthier Y. Hydrodynamics and mass transfer characteristics in gas-liquid flow through a rectangular microchannel. *Chem Eng Sci*. 2007;62:2096–2108.

8. Hisamoto H, Saito T, Tokeshi M, Hibara A, Kitamori T. Fast and high conversion phase-transfer synthesis exploiting the liquid-liquid interface formed in a microchannel chip. *Chem Commun*. 2001;2662–2663.
9. Irandoust S, Ertlé S, Andersson B. Gas-liquid mass transfer in Taylor flow through a capillary. *Can J Chem Eng*. 1972;70:115–119.
10. Kreutzer MT. Hydrodynamics of Taylor Fflow in Capillaries and Monolith Reactors. Delft University of Technology, Delft, The Netherlands; 2003. PhD. Thesis.
11. van Baten JM, Krishna R. CFD simulations of mass transfer from Taylor bubbles rising in circular capillaries. *Chem Eng Sci*. 2004; 59:2535–2545.
12. Kockmann N, Kiefer T, Engler M, Woias P. Convective mixing and chemical reactions in microchannels with high flow rates. *Sens Actuators B*. 2006;117:495–508.
13. Di Miceli Raimondi N, Prat L, Gourdon C, Cognet P. Direct numerical simulations of mass transfer in square microchannels for liquid-liquid slug flow. *Chem Eng Sci*. 2008;63:5522–5530.
14. Mary P, Studer V, Tabeling P. Microfluidic droplet-based liquid-liquid extraction. *Anal Chem*. 2008;80:2680–2687.
15. Tsoligkas AN, Simmons MJH, Wood J, Frost CG. Kinetic and selectivity studies of gas-liquid reaction under Taylor flow in a circular capillary. *Catal. Today*. 2007;128:36–46.
16. Sarrazin F, Prat L, Di Miceli N, Cristobal G, Link DR, Weitz DA. Mixing characterization inside microdroplets engineered on a microcoalescer. *Chem Eng Sci*. 2007;62:1042–1048.
17. Vandu CO, Liu H, Krishna R. Mass transfer from Taylor bubbles rising in single capillaries. *Chem Eng Sci*. 2005;60:6430–6437.
18. Deckwer WD. *Mass Transfer and Reaction*. In: *Bubble Column Reactors*. Chichester: John Wiley & Sons, Inc; 1992;47–68.
19. Legendre D, Magnaudet J. The lift force on a spherical bubble in a viscous linear shear flow. *J Fluid Mech*. 1998;368:81–126.
20. Tryggvason G, Bunner B, Esmaeeli A, Juric D, Al-Rawahi N, Tauber W, Han J, Nas S, Jan YJ. A front-tracking method for the computation of multiphase flow. *J Comput Phys*. 2001;169:708–759.
21. Koynov A, Khinast JG, Tryggvason G. Mass transfer and chemical reactions in bubble swarms with dynamic interfaces. *AIChE J*. 2005; 51(10):2786–2800.
22. Benkenida A, Magnaudet J. Une méthode de simulation d'écoulements diphasiques sans reconstruction d'interfaces. *C R Acad Sci Série IIb*. 2000;328(1):25–32.
23. Sarrazin F, Loubière K, Prat L, Gourdon C, Bonometti T, Magnaudet J. Experimental and numerical study of droplets hydrodynamics in microchannels. *AIChE J*. 2006;52(12):4061–4070.
24. Yang C, Mao ZS. Numerical simulation of interphase mass transfer with the level set approach. *Chem Eng Sci*. 2005;60:2643–2660.
25. Kashid MN, Agar DW, Turek S. CFD modelling of mass transfer with and without chemical reaction in the liquid-liquid slug flow microreactor. *Chem Eng Sci*. 2007;62:5102–5109.
26. Roizard C, Wild G, Charpentier JC. Absorption avec réaction chimique. *Tech Ing Genie Procedes*. 1997;J;1079.
27. Last W, Stichlmair J. Determination of mass transfer parameters by means of chemical absorption. *Chem Eng Technol*. 2002;25:385–391.
28. Danckwerts PV. *Gas-Liquid Reactions*. New York: Mc Graw-Hill, Inc; 1970.

*Manuscript received Mar. 5, 2009, and revision received July 29, 2010.*